

A two-dimensional Kolmogorov–Smirnov test for crowded field source detection: *ROSAT* sources in NGC 6397

S. A. Metchev¹ and J. E. Grindlay²

¹Department of Astronomy, California Institute of Technology, Pasadena, CA 91125, USA

²Harvard-Smithsonian Centre for Astrophysics, 60 Garden Street, Cambridge, MA 02138, USA

29 October 2018

ABSTRACT

We present a two-dimensional version of the classical one-dimensional Kolmogorov–Smirnov (K-S) test, extending an earlier idea due to Peacock (1983) and an implementation proposed by Fasano & Franceschini (1987). The two-dimensional K-S test is used to optimise the goodness of fit in an iterative source-detection scheme for astronomical images. The method is applied to a *ROSAT*/HRI x-ray image of the post core-collapse globular cluster NGC 6397 to determine the most probable source distribution in the cluster core. Comparisons to other widely-used source detection methods, and to a *Chandra* image of the same field, show that our iteration scheme is superior in measuring statistics-limited sources in severely crowded fields.

Key words: methods: data analysis – methods: statistical – globular clusters: individual (NGC 6397) – x-ray: stars

1 INTRODUCTION

Deep x-ray imaging of crowded fields, even with increasing angular resolution and sensitivity (with *Einstein* and *ROSAT*, and now *Chandra*), is invariably limited by the small number of source counts and by the relative size of the point-spread function (PSF) compared to the angular separation between the objects. Determining the underlying source configuration in such a regime is often beyond the capabilities of conventional source-finding algorithms.

Classical x-ray source detection methods are based on a sliding detection cell of a fixed size across the image, and calculating the signal-to-noise ratio (*S/N*) at each step. To find *S/N*, common detection algorithms for processing data from *Einstein* and *ROSAT* (implemented in *IRAF*¹/PROS²) use either an average background (as determined from a source-free section of the image) or a local background (from a region around the detection cell). However, both methods fail to discern blended faint sources in crowded fields where the background is affected by overlapping PSFs. Source detection is somewhat improved by image deconvolution, e.g. with the Lucy–Richardson (L-R) algorithm or with the Maximum Entropy Method (MEM), or by wavelet smoothing. Deconvolution algorithms provide higher positional sensitivity in moderately crowded

fields, but suffer from such undesirable effects as noise-amplification and “leakage” (associating counts from fainter sources to brighter nearby ones). Wavelet detection implemented as task WAVDETECT in the *Chandra* processing package (available at <http://asc.harvard.edu/ciao>) does well in crowded fields, provided the sources are either sufficiently separated ($\gtrsim 3\text{--}5$ FWHM, or $\gtrsim 3\text{--}5$ arcsec) or within $\sim 2\text{--}3$ FWHM and are similar in flux (Damiani et al. 1997; Freeman et al. 2001). When the PSFs are heavily blended (separation between the source centroids $\lesssim 1.5$ FWHM), individual sources cannot be distinguished and their relative fluxes cannot be measured. A superior source-detection method is needed for severely crowded fields containing multiple faint sources, e.g. globular cluster cores (Hertz & Grindlay 1983), or nuclear bulges in external galaxies.

A powerful technique to compare statistics-limited samples is the Kolmogorov–Smirnov (K-S) test which, unlike its alternative – the Pearson χ^2 test – does not require binning of the data. Unfortunately, the classical K-S test is applicable only to one-dimensional distributions, and any attempts to convert a two-dimensional image to one dimension (e.g. by collapsing it onto a vector, or by azimuthal binning around a point) lead to unwanted loss of information and power. For some time now, a multi-dimensional version of the K-S test has been known (Peacock 1983; Gosset 1987), which performs better than the χ^2 test in the small-number statistics case (Fasano & Franceschini 1987, hereafter, FF), and can be successfully applied in parameter point estimation in a manner similar to the widely used maximum-likelihood (ML) method. These properties of the multi-dimensional K-

¹ Image Reduction and Analysis Facility; developed and maintained by the National Optical Astronomy Observatories.

² Post-Reduction Off-line Software; developed and maintained by the Smithsonian Astrophysical Observatory.

S test make it viable for incorporation in source-detection methods.

In this paper, we re-visit the characteristics of the K-S test in two (and three) dimensions and examine its power in comparing different realisations of crowded low S/N fields. As an application of the test, we devise an iterative source-modelling scheme that aims to minimise the K-S statistic in search of the optimum underlying source distribution in an image. Based on our Monte Carlo simulations, we find that our iterative algorithm is a powerful tool for faint object searches in crowded fields. We apply the algorithm to determine the faint x-ray source distribution in a deep *ROSAT* exposure of the post core-collapse globular cluster NGC 6397, which has also been analysed with ML techniques by Verbunt & Johnston (2000). We compare the derived x-ray positions with those of Verbunt & Johnston and with our subsequent optical (*HST*, Taylor et al. 2001) and x-ray (*Chandra*, Grindlay et al. 2001a) identifications.

2 THE TWO-DIMENSIONAL K-S TEST

2.1 Description

The classical one-dimensional (1D) K-S test makes use of the probability distribution of the quantity D_{KS} , defined as the largest absolute difference between the cumulative frequency distributions of the parent population and that of an n -point sample extracted from it. Since D_{KS} is approximately proportional to $1/\sqrt{n}$, one usually refers to the probability distribution of the quantity $Z_n \equiv D_{KS}\sqrt{n}$. For a given n , the values of Z_n corresponding to a given significance level SL (denoted as $Z_{n,SL}$) increase slightly with n . For large n , the integral probability distribution $P(>Z_n) = 1 - SL$ approaches the asymptotic expression (Kendall & Stuart 1979):

$$P(>Z_n) = 2 \sum_{k=1}^{\infty} (-1)^{k-1} \exp(-2k^2 Z_n)$$

which is satisfactory for $n \geq 80$. For the two-sample K-S test, which compares distributions of different sizes (n_1 and n_2), the probability distribution $P(>Z_n)$ remains unchanged provided that n is set to $\frac{n_1 n_2}{n_1 + n_2}$. The 1D nature of the test implies that it does not depend in any way on the shape of the parent distribution.

In a two-dimensional (2D) distribution, each data point is characterised by a pair of values, (x, y) . As with the 1D K-S test, the maximum cumulative difference between two 2D distributions is found over the (x, y) -plane. In the case of distributions in more than one dimension however, the procedure to cumulate the information onto the plane is not unique. FF made use of the total number of points in each of the four quadrants around a given point (x_i, y_i) , namely, the fraction of data points in the regions $(x < x_i, y < y_i)$, $(x < x_i, y > y_i)$, $(x > x_i, y < y_i)$, $(x > x_i, y > y_i)$. The 2D statistic D_{KS} is defined as the maximum difference between data fractions in any two matching quadrants of the sample and of the parent population, ranging over all data points. The Z_n statistic is defined similarly as in the 1D case, $Z_n \equiv D_{KS}\sqrt{n}$, where for a two-sample 2D K-S test $n \equiv \frac{n_1 n_2}{n_1 + n_2}$.

Based on their Monte Carlo simulations, FF deduce that the 2D integral probability distribution $P(>Z_n)$ de-

pends solely on the correlation coefficient (CC) of the model distribution, i.e. that for a given CC the distribution of Z_n in the 2D K-S test is (nearly) independent of the shape of the model, as in the classical 1D K-S test. FF also observe that in the two-sample case, it is sufficient to take the average of the correlation coefficients CC_1 and CC_2 of the samples as an estimate of CC .

An important distinction between Peacock's and FF's version of the 2D K-S test was pointed out to us by the referee, which makes the latter generally less stringent. FF restrict the search for the maximum cumulative difference D_{KS} to loci harbouring a data point, thereby often missing the location of the true maximum difference, which is almost always found for $(x < x_i, y < y_j)$, where i and j are two different data points. Nevertheless, the maximum cumulative difference computed in such a way will have a tendency to vary in the same manner as the true maximum difference. Thus the FF statistic is probably well-behaved, at least as long as the genuine parent population distribution and the assumed one are not too different (Gosset 1987). The latter situation is indeed expected when comparing distributions of point-spread functions in two images. The advantage of FF's approach is speed: order n , instead of n^2 . The disadvantage is its approximate nature and that the D_{KS} statistic is sensitive to the correlation coefficient CC of the distributions, requiring its inclusion as a free parameter in the reference tables. Our Monte Carlo experiments below take into account both factors.

2.2 Monte Carlo experiments

Following the procedure in FF, we used the 2D K-S test computer code provided in *Numerical Recipes* (Press et al. 1997) to run our own Monte Carlo experiments. We studied the Z_n statistic by means of a Monte Carlo procedure using a uniform distribution ($CC = 0$) within the unit square as a parent population. The analysis comprised of cases with number of points n per sample ranging from $n = 5$ to $n = 50000$. For any given n we produced a large number of simulations (from 100000 for $n = 5$ to 1000 for $n = 50000$), enabling us to construct the integral probability distribution $P(>Z_n)$ with sufficient accuracy. Values of $Z_{n,SL}$ for uniform samples of all tested sample sizes n are listed in Table 1.

Figure 1 presents a comparison between our and FF's results for the critical values $Z_{n,SL}$ as a function of n . Both sets of Monte Carlo simulations show similar tendencies in the behaviour of the Z_n statistic, and are indistinguishable from each other for $n \geq 500$ within the statistical uncertainties (≈ 5 per cent for high n , due to the limited number of simulations). There is however a marked inconsistency between the two sets of data in the low- SL , small- n part of the graph, where at the 30 per cent significance level, the values of $Z_{n,SL}$ differ by a factor of ~ 1.15 . The difference is highly significant, given the fact that both FF's and our results for small n are based on 100000 simulations. We attribute this discrepancy to a detail in the implementation of the 2D K-S test: in particular, to whether the data point around which the D_{KS} statistic is computed, is included in one of the cumulative quadrants or not. This discrepancy becomes irrelevant, when the same implementation of the 2D K-S test is used in both building the reference tables for the critical

Table 1. Critical values $Z_{n,SL}$ for a uniform uncorrelated distribution.

n^{\ddagger}	# of simul.	$SL(\%)^{\dagger}$	30	40	50	60	70	80	90	95	99
			30	40	50	60	70	80	90	95	99
5	100000	0.76	0.82	0.88	0.95	1.03	1.13	1.27	1.38	1.62	
10	100000	0.79	0.85	0.92	0.98	1.06	1.15	1.29	1.41	1.65	
20	100000	0.85	0.91	0.97	1.03	1.10	1.20	1.33	1.45	1.69	
50	100000	0.91	0.97	1.04	1.10	1.18	1.27	1.41	1.53	1.78	
100	10000	0.96	1.02	1.08	1.15	1.22	1.32	1.45	1.57	1.81	
200	5000	1.01	1.07	1.13	1.19	1.27	1.37	1.51	1.62	1.86	
500	5000	1.06	1.12	1.18	1.25	1.33	1.43	1.57	1.68	1.91	
1000	5000	1.09	1.15	1.21	1.28	1.35	1.45	1.60	1.73	1.98	
2000	5000	1.11	1.17	1.24	1.30	1.38	1.47	1.61	1.74	1.99	
5000	2000	1.14	1.21	1.27	1.34	1.42	1.50	1.64	1.74	1.96	
10000	1000	1.15	1.22	1.28	1.35	1.43	1.54	1.69	1.82	2.13	
20000	1000	1.14	1.21	1.29	1.37	1.45	1.56	1.74	1.89	2.20	
50000	1000	1.16	1.24	1.32	1.40	1.50	1.60	1.78	1.91	2.19	

[†]Significance level ($SL \equiv 1 - P(> Z_n)$).

[‡]Size of sample.

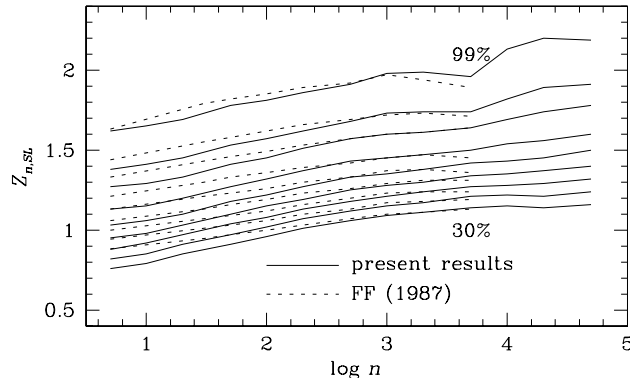


Figure 1. Critical values of the statistic Z_n as a function of sample size n , for values of the significance level SL varying from 30 per cent to 99 per cent. The continuous lines are based on data listed in Table 1, and the dashed lines are based on data reported in Table A1 of FF.

values of Z_n , and in comparing actual distributions using these tables.

3 USING THE TWO-DIMENSIONAL K-S TEST ON ASTRONOMICAL IMAGES

FF applied a 2D K-S test to astronomical distributions (not images) and showed that it can reject wrong hypotheses at a much higher significance level than the χ^2 test. We extend the application of the 2D K-S test to comparing images of crowded fields, where it is of great interest to determine whether a proposed source distribution corresponds to the observed one. When the PSFs of the individual sources are heavily blended (source separation $\lesssim 1.5$ FWHM), classical x-ray source-detection methods fail to distinguish the individual objects. Crowded-field optical photometry tools (e.g. DAOPHOT, Stetson 1987, 1991) are also not suitable for the small-number Poisson statistics of x-ray images. Even the recently introduced detection algorithm based on wavelet transforms (Freeman et al. 2001; Damiani et al. 1997, and references therein) implemented in the *Chandra* x-ray data

analysis package (CIAO³), does not produce adequate results in the regime of severe source confusion and small number of counts per source.

Below we describe an implementation of the 2D K-S test to astronomical images. Provided that the PSF of the (unresolved) sources in a crowded field is known and constant over the image, by comparing the image to a simulation of a proposed source distribution, we can obtain the K-S probability $P(> Z_n)$ that the image and the simulation represent the same source configuration. The obtained probability can be used as a measure of the accuracy of both the positions and the intensities of the proposed sources, as well as an indication of the necessity for additional sources to account for the photon distribution. Because of the high sensitivity of the 2D K-S test, we expect that it should be able to discern positional discrepancies equal to a fraction of the FWHM of the PSF.

3.1 Implementation of the two-dimensional K-S test

3.1.1 A two-dimensional vs. a three-dimensional K-S test

Astronomical images (e.g. from CCDs) have three dimensions: x and y pixel coordinates, and pixel intensity. Although the spatial distribution of photons that strike the detector is two-dimensional (two photons never fall at the exact same position), they are binned by the detector in integer bins corresponding to the digital pixel size. Thus the incoming 2D distribution of photons with real-valued coordinates is transformed into a three-dimensional (3D) one with integer coordinates. It is possible to apply the 2D K-S test to an integer-valued 3D distribution by simply re-calculating the two-dimensional D_{KS} statistic for every count in a given pixel. However, since the K-S test is designed to deal with real-valued distributions, any point in the (x, y) plane that has more than one count at the exact same real-valued position (which would be the case if a pixel contained more

³ *Chandra* Interactive Analysis and Observations; developed and maintained by the *Chandra* X-ray Center, and available at <http://asc.harvard.edu/ciao>.

than one count) becomes disproportionately significant, and distorts the value of D_{KS} .

Therefore, to apply a 2D K-S test to 3D images, it is first necessary to “un-bin” the images by spreading the counts in each pixel over the area of the pixel. Since no information is preserved about the exact impact locations of the photons on the detector, we introduce a random shift (between -0.5 and $+0.5$ pix) in the integer-valued coordinates of each count. Every count in the image is thus assigned a unique position (within the precision limits of the computer), and the integer-valued 3D coordinates are converted to real-valued 2D coordinates. Since this routine distributes the data on a sub-pixel scale, we refer to it as “subpixelization.”

Unfortunately, subpixelization incurs an undesirable effect, due to the randomness with which the counts are moved around within the pixels. In particular, two subpixelized versions of the same image are never the same. Therefore, K-S testing of different subpixelizations of the same two images will produce different results for Z_n every time. Our experience is that Z_n varies by about 2 to 4 per cent between runs; the corresponding variations in the significance level SL may be as high as ± 8 per cent for values of Z_n near $SL = 50$ per cent (Table 1). To obtain a mean value for the K-S probability $P(>Z_n)$ (equal to $1 - SL$) with which two images represent the same parent distribution, it is necessary to run the 2D K-S test multiple times. The error in the K-S probability can be estimated from the variations in Z_n among the different runs.

The above method may appear contrived and unnecessary, when instead of applying a 2D K-S test, by following the generalisation in FF, a 3D K-S test can be implemented. A 3D test does not have the undesirable uncertainties associated with subpixelization, and gives the exact K-S probability that two images represent the same parent distribution. FF report that the 3D test exhibits greater power in rejecting wrong hypotheses than a three-fold 2D test along each of the (x, y) , (y, z) and (z, x) planes. However, our experiments with the tests on simulated *ROSAT* images show that the 2D K-S test applied to subpixelized images is more powerful than its 3D counterpart (with accordingly generated look-up tables) applied to the original (not subpixelized) images. K-S tests performed on simulations of an 880-count five-source distribution with centre-to-centre distances of 1.1–2.1 times the PSF size (5 arcsec for *ROSAT/HRI*) show that the 2D test on subpixelized images can distinguish individual source position shifts as small as 2–3 arcsec (depending on the relative source locations and intensity) at the $\gtrsim 97$ per cent significance level. The 3D test finds such shifts insignificant: it gives a probability of $\gtrsim 70$ per cent that the simulations represent the same parent distribution.

The higher power of the subpixelized 2D test is explained by the manner in which pixels are weighted. Subpixelization ensures that all photons are assigned equal weights: a desirable effect, since pixels are weighted proportionally to their intensity. The 3D K-S test, on the other hand, assigns equal weights to all pixels, so single-count pixels (often from background) are as significant as pixels with multiple counts (denoting sources). Hence, the 2D test on subpixelized images is more sensitive to variations in the source distribution than its 3D counterpart.

We also note that subpixelized images represent more realistically the incoming photon distribution. Repeated 2D

K-S tests on independent subpixelizations produce an estimate of the random error in the K-S probability induced by photon binning.

3.1.2 One-sample vs. two-sample two-dimensional K-S test

When comparing an image to a proposed model distribution of sources (using an analytical or a fitted PSF), perfect information is available about the shape of the model distribution. It is therefore appropriate to use a one-sample K-S test to compare the image to the model distribution. However, the analytical form of a fitted PSF is often very complex. The added complication of having several nearby sources with overlapping PSFs (as in a crowded field) makes it computationally very tedious to calculate the fraction of the analytic model distribution in the quadrants around every count in the image (needed to compute the D_{KS} statistic; Section 2.1).

To avoid lengthy 2D surface integrals, the two-sample K-S test can be used instead, to compare the image to a simulation generated from the proposed model. The random deviations in the representation of the model can be decreased if a “bright” (high number of counts n) simulation is used, that follows the model closely. The fractional deviation of the simulated vs. expected counts per pixel will decrease as $1/\sqrt{n_{cts}}$ for large n_{cts} , where n_{cts} is the number of counts per pixel in the model image. The running time of the two-sample 2D K-S test is however proportional to the square of the sum $n_1 + n_2$ of counts in the samples compared, and it is impractical to use the two-sample K-S test on simulations containing high number of counts.

To take advantage of the higher power of the one-sample test (given perfect information about the shape of the model distribution), and to avoid long running time, we compare the image (containing n counts) to a bright simulation ($n_{mod} = k \times n$ counts; $k \sim 50$) of the proposed model, using the one-sample test. In essence, we use Monte Carlo integration for the model, the assumption being that a bright simulation can be made to represent the model with sufficient accuracy, and simple summing of the counts in the quadrants can be substituted for analytic integration of the PSF. We therefore do not expect the properties of this *pseudo* one-sample K-S test to be significantly different from those of the FF one-sample K-S test. In particular, we assume that the new test is still distribution-free for a fixed correlation coefficient CC of the bright simulation (hereafter referred to as the “model”), and that its properties vary slowly with CC (as observed in FF for their 2D K-S test). Clearly, our test will converge to the FF one-sample test for $k \rightarrow \infty$, but will run faster than the latter for moderate-sized k , since lengthy analytical integrations are substituted with Monte Carlo integration. The *pseudo* one-sample test (running time proportional to $n(n + n_{mod}) = (k + 1)n^2$) is also $k + 1$ times faster than the two-sample test (running time proportional to $(n + n_{mod})^2 = (k + 1)^2 n^2$). Thus, for moderate-sized k , the *pseudo* test approximates the power of the one-sample K-S test, and is faster than both the one-sample and the two-sample K-S tests for a general model distribution.

Table 2 presents a comparison of the performance of the two versions of the test, using the same five-source

Table 2. Comparison of the performance of the pseudo one-sample 2D K-S test and the FF two-sample K-S test as a function of $k = \frac{n_2}{n_1}$ for a model with $CC = 0.10$.

		pseudo one-sample test		two-sample test	
k	n_1	$Z_{n,1s}^a$	$P(> Z_n)$	\bar{n}^b	$Z_{n,2s}^a$
1	880	1.78 ± 0.07		440	1.30 ± 0.04
2	880	1.72 ± 0.05		587	1.44 ± 0.03
5	880	1.56 ± 0.04		733	1.48 ± 0.04
10	880	1.88 ± 0.05		800	1.79 ± 0.03
20	880	1.59 ± 0.06	$\lesssim 4\%^d$	838	1.64 ± 0.03
50	880	1.62 ± 0.04	$\lesssim 2\%^d$	863	1.65 ± 0.05
100	880	1.62 ± 0.06		871	1.68^e
200	880	1.66 ± 0.06		876	1.74^e

^a Errors determined from K-S comparisons of 10 different subpixelizations of the same simulations. Systematic uncertainties associated with representing a continuous model by a discrete distribution are not included.

^b For the two-sample test $\bar{n} = \frac{n_1 n_2}{n_1 + n_2} = \frac{k n_1^2}{n_1 + k n_1} = \frac{k}{k+1} n_1$.

^c Obtained from Table 1 for $CC = 0.10 \approx 0.0$ of the two samples.

^d Interpolated from lines 1 ($k \approx 50$) and 2 ($k = 25$) of Table 3 ($CC = 0.10 \approx 0.12$).

^e Only one comparison was performed due to the longer running time.

Table 3. Critical values $Z_{n,SL}$ for simulated source distributions. Model size $n_{\text{mod}} = 45000 \approx 50 \times 880$, i.e. $k \approx 50$.

CC	n^{\ddagger}	$SL(\%)^{\dagger}$	30	40	50	60	70	80	90	95	99
0.12	880	10000	0.98	1.03	1.08	1.13	1.20	1.27	1.38	1.47	1.67
0.12	1800	10000	1.03	1.08	1.13	1.19	1.24	1.32	1.43	1.54	1.74
0.23	820	10000	0.95	1.00	1.05	1.09	1.15	1.22	1.33	1.43	1.61
0.23	1800	10000	1.02	1.07	1.11	1.17	1.23	1.30	1.42	1.52	1.71

[†] Significance level ($SL \equiv 1 - P(> Z_n)$).

[‡] Size of sample.

setup as in Section 3.1.1, with one source shifted by only 0.4 FWHMs = 4 pix between the model and the simulations. As expected, the power of the two-sample test increases with increasing k , but for $k \geq 20$ the results for $Z_{n,2s}$ do not change significantly. The values of $Z_{n,1s}$ from the pseudo one-sample test exhibit greater random variations for small k than those of $Z_{n,2s}$. These are due to the fact that the small-number statistical uncertainties in the two samples are not averaged out in the one-sample test, whereas in the two-sample test they are. For $k \geq 20$ however, the values for $Z_{n,1s}$ become self-consistent (as well as consistent with those from the two-sample test), and there is little power to be gained from increasing k .

Despite the similar behaviour of the FF K-S test and our pseudo one-sample test, the reference tables for the former (Tables A1–A5 in FF; Table 1) cannot be used for the latter, since the Z_n distributions are different. We therefore ran Monte Carlo simulations to create a separate look-up table for the new test. Table 3 is based on comparing simulated source distributions with $n_1 \approx 850$ counts to $k \approx 50$ times brighter simulations (“models,” $n_2 \approx 45000$) of the same source distributions. Sources were simulated on a 128×128 pix field using the analytic 5-arcsec (10-pix) HRI PSF. We also ran Monte Carlo simulations with higher n_1 ($n_1 \approx 1800$) against $n_2 \approx 45000$ -count models for the purpose of interpolation. Although in this case the value of k is lower ($k = 25$), we choose to set the value of $n_2 = 45000$ as the standard, as it is a measure of the precision of the Monte Carlo integration. High values of the sample corre-

lation coefficient CC were not pursued, since astronomical images rarely have highly correlated photon distributions (esp. in crowded fields, but also given random background). Thus constructed, Table 3 should be applicable to most low background, low S/N imaging cases (esp. x-ray).

Using Table 3 for the values of $Z_{n,SL}$, the results for the K-S probability ($P > Z_n$) from the pseudo one-sample K-S test will be consistent with those from the FF K-S test using the FF tables. Hereafter, unless explicitly stated otherwise, we shall refer to our pseudo one-sample 2D K-S test as “the 2D K-S test,” or simply as “the K-S test.”

3.2 Application of the two-dimensional K-S test to simulated images

After establishing that the 2D K-S test can be successfully applied to images, it is important to determine the sensitivity of the test with respect to deviations from the proposed model. Here we test the responsiveness of the 2D K-S test with respect to changes in the parameters of individual sources in the model distribution. We look for the minimum deviation in a single parameter (position or intensity of a source) that enables the test to tell the distributions apart at the $\gtrsim 99$ per cent significance level. As a trial source distribution we use the one simulated in Figure 2a, whose parameters are listed in Table 4 (sources X1–X5), and compare it to models that have one parameter changed.

It is worth noting here, that given the significant overlap of PSFs in a crowded field such as the one in Figure 2a,

Table 4. Parameters of the source distribution best describing the x-ray emission in the central 128×128 pix section of the NGC 6397 *ROSAT* image.

Source	Pixel coordinates ($x - 4012$)	Pixel coordinates ($y - 4027$)	Counts	Counts ($\times 50$)
X1	71	55	78	3900
X2	56	56	176	8800
X3	59	37	161	8050
X4	73	39	88	4400
X5	76	88	197	9850
X6	94	77	16	800
bkg			0.015 cts/pix	0.75 cts/pix

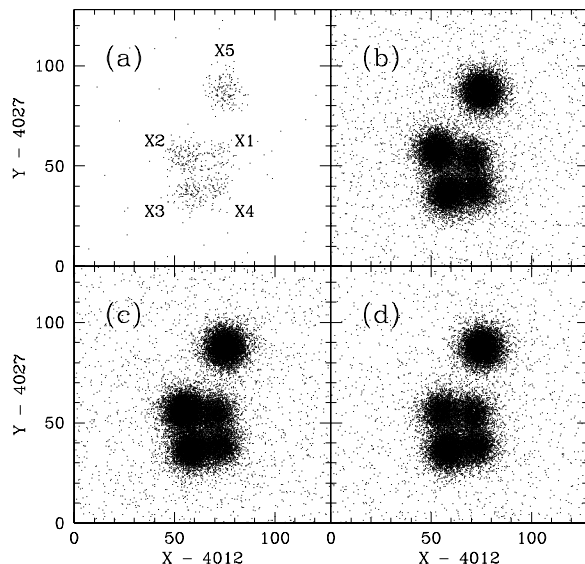


Figure 2. Scenarios for determining the sensitivity of the pseudo one-sample K-S test with respect to changes in the parent distribution. The x - and y -axes are HRI pixels. A 10-pixel FWHM PSF has been used. (a) A subpixelized 880-count 5-source simulation. The source parameters are listed in Table 4 (X1–X5). The simulations in (b)–(d) are 50 times brighter with a single source modified in each: (b) source X2 is moved 2 pix up and 2 pix to the left; (c) source X2 is 1.45 times brighter (11600 cts); (d) source X2 is at 60 per cent intensity (4800 cts).

the sensitivity of the test with respect to changes in the distribution need not be isotropic. It depends on the relative positioning and brightness of the sources. We therefore test several possible scenarios of such changes. The scenarios shown in Figure 2 and described in its caption correspond to the limiting cases, in which the K-S test can distinguish the distributions at the $\gtrsim 99$ per cent level.

After performing K-S tests between the simulation in Figure 2a and the models in Figures 2b–d, we establish that the positional sensitivity of the K-S test in crowded fields depends on the relative source intensity, and on the direction in which a source is allowed to move with respect to the crowded region. The sensitivity to moving a source is higher for brighter sources (3 to 4 pix for source X2) than for the fainter ones (4 to 9 pix for source X1), and is generally (although not conclusively) poorer when the source is moved toward the region of crowding (9 pix for source X1, 3 pix for X2) as opposed to when it is moved away (4 pix for X1 and X2). The brightness sensitivity of the K-S test is also

Table 5. Number of sources in the best-fit model vs. K-S probability.

N	CC of model	Z_n	K-S prob $P(> Z_n)^a$	P'_N ^b
3	0.21	1.88 ± 0.04	< 1%	1.5%
4	0.22	1.48 ± 0.05	4 \pm 1%	43%
5	0.19	1.23 ± 0.05	22 \pm 6%	90% ^c
6	0.21	1.19 ± 0.04	26 \pm 6%	(100%)

^a For $n = 980$ counts in the NGC 6397 image.

^b Probability that a best-fit model with N sources and the *ROSAT* image represent the same parent distribution; $1 - P'_N$ is the significance of adding an $(N + 1)$ -st source. P'_N is calculated as $P_{N,5}$ (Section 7.2).

^c Estimated as $P_{5,6}$, i.e. the probability that a 5-source best-fit distribution can represent a 6-source one; $1 - P_{5,6} = 10$ per cent is the significance of adding a sixth source.

dependent on the relative source intensity in a crowded field: brighter sources can vary by a smaller percentage (~ 45 per cent for X2) than fainter sources (~ 70 per cent for X1). For a source that is sufficiently far away (~ 3 FWHM) from the crowded region (source X5) the sensitivity of the K-S test is greater and nearly position-independent. For source X5 we set the limits at a 2 pix shift in any direction ($P(> Z_n) \approx 1$ per cent) or a 30 per cent change in intensity ($P(> Z_n) < 1$ per cent).

The above-determined sensitivity limits are based on varying only one parameter (position or intensity) of a single source, while keeping all other parameters fixed. This is the approach used to determine the 95 per cent ($\approx 2\sigma$) confidence limits (Table 6) on the positions and intensities of the detected sources in our NGC 6397 image (Section 5).

4 THE 2D K-S TEST IN PARAMETER POINT ESTIMATION FOR SOURCE DETECTION

4.1 Algorithm

An iterative source-fitting algorithm was devised that aims to minimise the Z_n statistic, thus maximising the probability that an image and a simulation represent the same parent distribution of sources. The final simulation that results from this algorithm will contain the best estimate for the number, positions and intensities of the sources in the image, subject to limitations arising from the sensitivity of the test. The iterative procedure steps through the following algorithm:

(i) An initial guess of the source distribution is made. This can be a source at the location of the brightest pixel (thus starting with a one-source configuration) or a guess with $N_{\text{initial}} > 1$ number of sources. Both initial guesses will produce the same results for a distribution with $N_{\text{final}} \geq N_{\text{initial}}$ sources. The PSF is fit to a single unresolved source in an uncrowded part of the image so that aspect or other image systematics are included.

(ii) A bright simulation (a.k.a. a “model”; see Section 3.1.2) based on the current guess for the source distribution is created (using the fitted PSF) and normalised to the image intensity. The normalised model and the image are smoothed with a Gaussian function to roughly match the *ROSAT*/HRI resolution. The residual between the two is then formed.

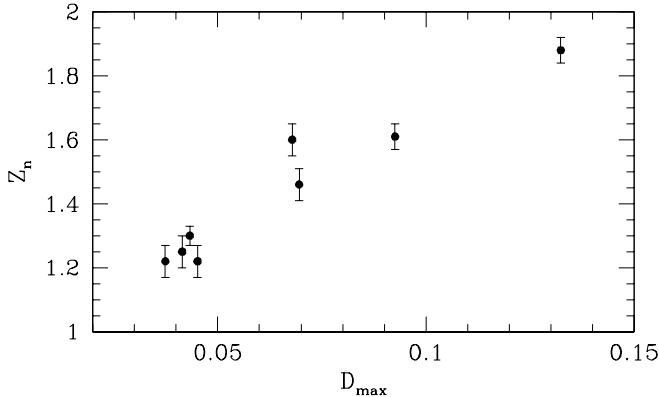


Figure 3. Values of Z_n vs. the maximum deviation from zero, D_{\max} , in the smoothed residual. The error-bars in Z_n represent the standard deviation of Z_n due to 10 independent subpixelizations of the compared simulations. The statistics Z_n and D_{\max} are highly correlated (correlation coefficient 0.93), and we therefore use a minimum in D_{\max} as an indication of being near a minimum in Z_n (and hence, for constant CC , near a maximum in $P(>Z_n)$).

(iii) The next guess for the source distribution is obtained by moving the source positions against the steepest gradient in the residual, and by adjusting the intensities, so as to decrease the maximum deviation from zero (D_{\max}) in the smoothed residual. We indeed observe that D_{\max} is strongly correlated to the value of Z_n (correlation is 0.93; Figure 3), and hence (for constant CC) to the K-S probability $P(>Z_n)$.

(iv) Repeat steps (ii) and (iii) until D_{\max} is minimised. Compare the image to the model with the 2D K-S test and, if necessary, further minimise Z_n by applying small changes (e.g. single-pixel shifts) to the model (since the nature of the relation between D_{\max} and Z_n is not established rigorously). The final simulation will contain the best guess of the positions and intensities of the assumed sources. The image is compared to the model using the 2D K-S test.

(v) Steps (i) through (iv) are run for a fixed number of sources (guessed in step (i)). If the final K-S probability of similarity is not satisfactory (e.g. not $\gtrsim 5$ per cent), a new source is added at the location of the highest residual, and the algorithm is repeated from step (ii).

(vi) If the addition of the last source did not incur a decrease in the Z_n statistic larger than its uncertainty (± 2 per cent to ± 4 per cent), the last added source is considered marginal, and the previous best guess for the number, positions and intensities is taken as the final one.

As noted in step (i) an initial guess with $N_{\text{initial}} > 1$ number of sources can also be fed into the algorithm. Such a guess can be made either from visual inspection of the image, or after applying a deconvolution algorithm. We found that L-R deconvolution (see Section 6 below) gives good initial estimates of the positions of the individual sources. However, since deconvolution can introduce spurious sources, the initial guess of the number of sources should be conservative.

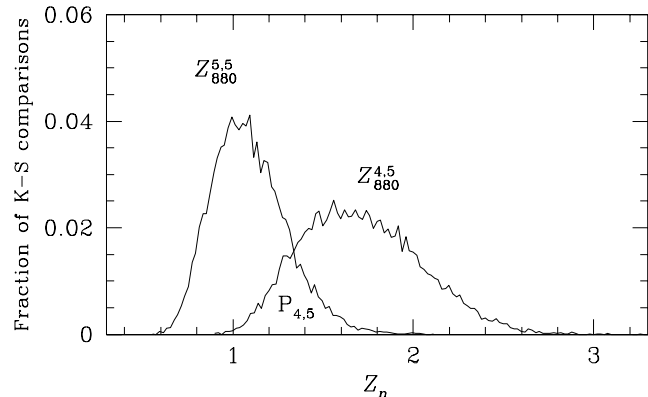


Figure 4. A comparison between a $Z_{880}^{5,5}$ and a $Z_{880}^{4,5}$ curve obtained using the 5-arcsec predicted HRI PSF. The $Z_{880}^{4,5}$ curve is obtained from K-S tests between a 5-source model and 10000 realisations of a 4-source simulation that best represents the 5-source model. The overlap area $P_{4,5}$ determines the false detection probability of the 5th source. Here $P_{4,5} = 0.23$.

4.2 Performance

The above procedure has not been automated, and therefore (due to subjectivity in “guessing” a simulated source distribution after having created it) we have not performed tests to explicitly determine its efficiency in detecting sources. We quote the ability of the 2D K-S test to detect small changes in the positions (within ~ 0.2 FWHM) and/or intensities of individual sources (Section 3.2) as an indication of the power of the iterative algorithm. Nevertheless, we have devised a method to test the confidence with which a certain number of sources can be claimed in a given photon distribution. The method takes our best guess for the source distribution in the image with a given number of sources (e.g. N), and compares a model of it to a faint simulation of our best guess with one source fewer ($N-1$). In this way we can test in what fraction $P_{N-1,N}$ of the cases our proposed model (with N sources) can describe a source distribution with $N-1$ sources. In other words, we test for the significance $(1-P_{N-1,N})$ of the addition the N -th source; $P_{N-1,N}$ is thus its false-detection probability. If this comparison is performed many of times (of the order of the number of Monte Carlo simulations done for each row in Table 3), a $Z_n^{N-1,N}$ curve for the two guesses is recovered. The latter can be then compared to a $Z_n^{N,N}$ curve, obtained in a similar fashion comparing N -source simulations to an N -source model.

Example $Z_n^{N,N}$ and $Z_n^{N-1,N}$ curves for $N = 5$ and $n = 880$ are shown in Figure 4. The overlap of the two curves gives the fraction of Monte Carlo simulations, in which a best-fit distribution with $N-1$ sources produces an image that has the same K-S similarity to the model as that of a best-fit distribution with N sources. The ratio of the overlap area to the area of either of the Z_n curves (assuming they are both normalised to the same area) is the desired fraction $P_{N-1,N}$.

To investigate the dependence of the overlap area $P_{N-1,N}$ on the width of the PSF, we ran K-S tests simulations built with an 8-arcsec Gaussian PSF. The result is that for a wider PSF the $Z_n^{N-1,N}$ curve is narrower and is shifted

toward smaller Z_n (the model and the simulations look more alike). The $Z_n^{N,N}$ curve however is not affected. The overall effect is that the false-detection probability $P_{N-1,N}$ of the N -th source increases (from 0.23 to 0.43 for $N = 5$; Table 5).

The above technique can be generalised to produce $P_{N-i,N}$ for arbitrary integers $i < N$ and j . An application of $P_{N-i,N}$ is discussed in Section 7.2.

5 APPLICATION TO A DEEP ROSAT IMAGE OF NGC 6397

The iterative source-modelling procedure (Section 4.1) was applied to our 75 ksec *ROSAT/HRI* exposure (March 1995) of the core region of the post core-collapse globular cluster NGC 6397 (Figure 5). Standard aspect correction routines (Harris et al. 1998a,b; Harris 1999a,b) were applied to the image to improve the S/N ratio. After the aspect corrections the PSF improved from $10.3 \text{ arcsec} \times 8.3 \text{ arcsec}$ to $8.3 \text{ arcsec} \times 7.9 \text{ arcsec}$, as measured from the shape of a background point-source quasi-stellar object (QSO) at 3.7 arcmin off-axis (source "D" in Cool et al. 1993). The obtained size of the PSF was still much worse than the predicted 5 arcsec. This effect is not due to the known deterioration of the *ROSAT* PSF with increasing off-axis angle beyond ~ 5 arcmin, since the QSO is only 3.7 arcmin from the centre of the field. Residual (unknown) aspect errors are present, and in the analysis below we use a fitted PSF instead of the nominal one.

We analyse the central 128 pixel (64-arcsec) square region of the image, containing 980 counts. Model simulations were created using an analytical PSF fit to the QSO with the *IRAF/DAOPHOT* routines PSF and ADDSTAR. The PSF was comprised of a $\text{FWHM} \approx 8\text{-arcsec}$ Gaussian core and Lorentzian wings, where the core and the wings could be tilted along different directions in the image. In determining the false-detection probabilities (from the overlap of the Z_n curves) however, for faster iteration we used a symmetrical 8-arcsec Gaussian PSF, noting that the Z_n distributions based on the fitted PSF and on the Gaussian PSF are expected to be indistinguishable, since the test is distribution-free.

Table 5 presents results for the K-S statistics of the best-fit models for a given number of sources. The error in the values of Z_n and $P(> Z_n)$ is the one-sigma uncertainty due to subpixelization, as determined from K-S comparisons between the model and 10 independent subpixelizations of the same image. It is an estimate of the error in the mean of the Z_n distribution of comparisons between the image and the N -source model.

Following the logic of step 6. in the K-S probability maximisation algorithm (Section 4.1), we conclude that four sources are insufficient to represent the image conclusively, since the addition of a fifth source decreases the Z_n statistic by more (17 per cent) than the 3.5 per cent error in the Z_n statistic for four sources. However, the addition of a sixth source is not justified, since the decrease (0.04) in Z_n is smaller than the error (0.05). We therefore claim that five sources are sufficient, and that at least four sources are necessary (at the $1 - P_{3,5} > 99$ per cent level) to account for the observed photon distribution in the *ROSAT* image. The source centroids for the optimal source configurations with

4, 5 and 6 sources are shown in Figure 6. The number of counts per source for the five- and six-source cases are the same as listed in Table 4.

Source X6 is sufficiently faint and detached from the central group (X1–X4), that its addition did not necessitate any changes in the prior five-source configuration. It is 11 arcsec away from the closest source (X1), and 4.5 times dimmer than the faintest one (also X1; Table 4). The false detection probability (determined as $P_{5,6}$) for source X6 is 90 per cent.

Source X_{1,4} in the four-source best-fit solution falls approximately in the middle between sources X1 and X4 of the five-source solution, which is consistent with them having comparable intensities and being fainter than X2 and X3 (Table 4).

The derived optimal number of five sources in our 75 ksec image of NGC 6397 is consistent with the earlier suggestion (Cool et al. 1993) that at least four x-ray sources (X1, X2, X3 and X5) are present in an 18 ksec exposure of the same region (found by visual inspection of the peaks in the image, and confirmed by a one-dimensional azimuthal K-S test around the source centroids). The locations of the detected sources are also consistent (up to a $\sim 2\text{-arcsec}$ systematic offset) with the positions of known optical cataclysmic variables (CVs): the optimum five-source positions (solid triangles, Figure 6) are systematically displaced by $\sim 2\text{ arcsec}$ to the lower right of CV1–CV5 (open triangles, as measured from $\text{H}\alpha$, \mathcal{R} , and *UBVI HST* data; Cool et al. 1995, 1998). Such an offset is well within the expected variation ($\lesssim 5\text{ arcsec}$) of the absolute pointing of *ROSAT*.

Source X5 does not have a known optical counterpart, and sources CV1 and CV4 are unresolved in the *ROSAT* x-ray image due to their proximity ($\sim 2.5\text{ arcsec} \approx 0.3\text{ FWHM}$), so that the emission of X1 is probably due to both of them. The object CV5 was previously known (Cool et al. 1998) as a near *UV*-excess star, but proposed as a CV-candidate (Grindlay 1999; Metchev 1999) only after re-evaluating its probable association with the x-ray emission from X4. Its subsequent confirmation as a CV-candidate ($\text{H}\alpha$ -emission object) in our followup deep *HST* imaging (Taylor et al. 2001) is indicative of the reliability of our iteration scheme to detect faint sources in crowded fields.

Similarly, source X6 (if real) may be associated with the *Chandra* source U43 (Grindlay et al. 2001a): a probable faint BY Draconis binary, identified as PC-4 in Taylor et al. (2001). Such objects are expected in globulars as the binary companions of stars on to which they have transferred their envelopes, and indeed the reported velocity in Edmonds et al. (1999) suggests a massive but dark binary companion. The latter is most likely a neutron star (NS), since He-WD/NS systems are expected in millisecond pulsars (MSPs), and MSPs are detected as faint x-ray sources with luminosities comparable to that of X6 (cf. Becker & Trümper 1999).

Table 6 lists results for the detected sources. A mean bore-sight offset of -3.5 ± 1.0 pix in x , and $+1.7 \pm 1.0$ pix in y (-1.8 arcsec and $+0.85\text{ arcsec}$, respectively) has been applied to the x-ray positions to align them with the suggested optical counterparts. In calculating the offset, we discard source X1 (since the x-ray emission in its vicinity comes most likely from both CV1 and CV4), and weigh the measured shifts inversely to the square of the positional uncertainties of the

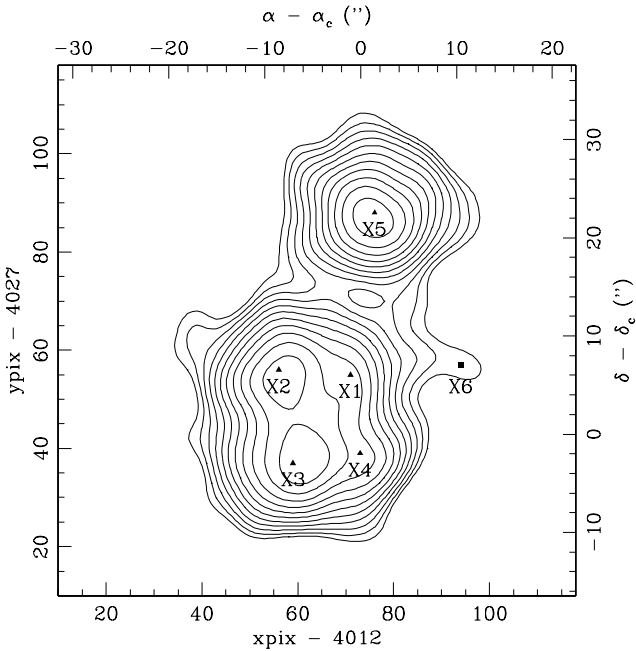


Figure 5. A 75 ksec *ROSAT*/HRI exposure of the central region of NGC 6397, with the detected sources marked. The x-ray image is smoothed with a 2-d $\sigma = 2$ arcsec Gaussian. The cluster centre is at $(\alpha_c, \delta_c) = (17:40:41.3, -53:40:25)$, (Djorgovski & Meylan 1993). The conversion from pixel to celestial coordinates is accurate to within 1 arcsec.

sources along x and y . The 95 per cent confidence radius of the source coordinates corresponds to the maximum shift of a single source from its listed position (keeping all intensities and other source positions constant) that maintains the K-S probability above 5 per cent.

6 COMPARISON TO OTHER SOURCE DETECTION METHODS

To get an idea of the superior performance of our source-modelling scheme we compared it to established source-detection algorithms, such as the classical “sliding-cell” detect, the wavelet detect, the *IRAF/DAOPHOT* PSF-fitting task *ALLSTAR*, and ML analysis. We also used deconvolution routines on the image to determine possible source locations. Below we discuss briefly each of these alternatives.

Sliding-cell Detect: The sliding-cell detect algorithm is based on S/N calculation and was not expected to perform well in a crowded low- S/N field. Indeed, the two versions of this algorithm in the *IRAF/PROS* package (tasks *IMDETECT* and *LDETECT* in the *XSPATIAL* package) fail to produce the expected number of x-ray sources in the cluster. *IMDETECT* uses a constant average background for the entire image, and a variable detect cell size (squares with sides from 4 arcsec to 24 arcsec) to search for sources. The larger detect cells fail to find more than three sources in the central region of NGC 6397, whereas the 4-arcsec detect cell size is too small for use with our PSF ($\text{FWHM} \approx 8$ arcsec), and produces an unjustified high number of individual sources. The local detect algorithm (task *LDETECT*) calculates S/N around each pixel, using the local background (in a region between

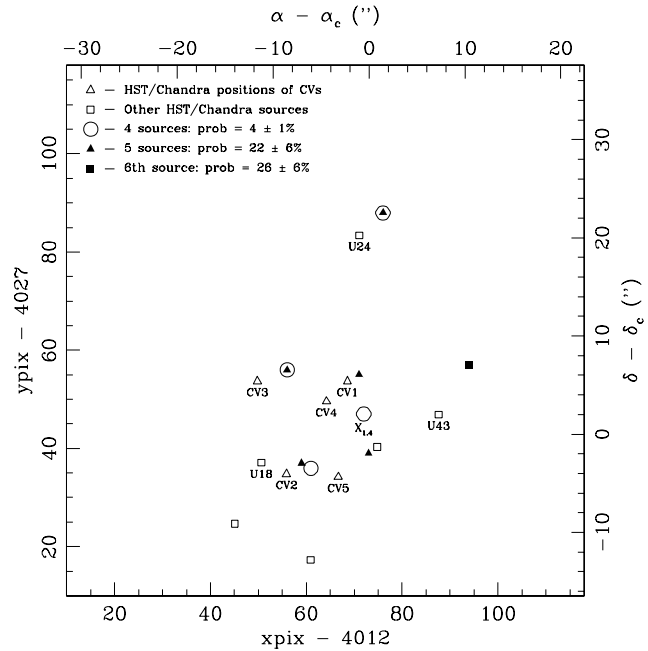


Figure 6. Best-fit source positions for 4, 5 and 6 sources. Open triangles mark the positions of known H α -emission objects (probable CVs, numbered with their ID from Cool et al. 1995; Grindlay 1999) – candidate counterparts for sources X1–X4. Open squares mark *UV*-excess (Cool et al. 1995; Edmonds et al. 1999) and/or faint ($L_x < 10^{31} \text{ erg s}^{-1}$) *Chandra* sources (IDs from Fig. 1 of Grindlay et al. 2001a). The consistent shift between the *HST/Chandra* CV and the *ROSAT* x-ray positions is indicative of a bore-sight offset (~ 2 arcsec) of *ROSAT* for this observation.

1.5 arcsec and 2.5 arcsec from the source) as an estimate of the noise. As a result it does not handle crowded fields adequately, and cannot distinguish blended sources. Even the two smallest detection cells (6 arcsec \times 6 arcsec and 9 arcsec \times 9 arcsec) do not find more than 3 sources in the image in Figure 5.

Wavelet Detect: This algorithm based on the wavelet transform has only recently been applied to imaging astronomy (Freeman et al. 2001; Damiani et al. 1997, and references therein), and has been demonstrated to outperform other source detection algorithms in low- S/N fields. We used an implementation of the wavelet detect based on the Marr wavelet, or the “Mexican Hat” function, coded in the *WAVDETECT* task in the *Chandra* *DETECT* 1.0 Package. The algorithm is most sensitive to structures of size approximately equal to the width of the Mexican Hat function. Running *WAVDETECT* on our NGC 6397 image (Figure 5) with transforms of width ≤ 8 arcsec produced only the same three sources already found by the sliding-cell algorithms. This was not unexpected, since in simulated images for the *Chandra* High Resolution Camera ($\text{FWHM} = 0.5$ arcsec), *WAVDETECT* is unable to discern point sources less than 2 FWHM apart.⁴

Image Deconvolution: There exist a number of widely used image deconvolution algorithms that are applicable to

⁴ *Chandra* *DETECT* User’s Guide; URL: <http://heawww.harvard.edu/asclocal/user/swdocs/detect/html/>

Table 6. X-ray sources detected in NGC 6397.

Source	R.A. (J2000)	DEC. (J2000)	95% conf. radius	Count rate (ksec ⁻¹)	L_x (erg/s) ^a $kT = 10$ keV	Optical counterpart ^c	<i>Chandra</i> offset ^d (arcsec)
X1	17:40:41.46	-53:40:18.4	2.5''	1.2 ± 0.5	3.3×10^{31}	CV1, CV4	$\alpha_R - \alpha_C$ -0.2
X2	17:40:42.48	-53:40:18.0	1.5''	2.7 ± 0.6	7.4×10^{31}	CV3	$\delta_R - \delta_C$ 0.7 1.2
X3	17:40:42.32	-53:40:27.4	1.5'' × 2.5''	2.5 ± 0.6	6.9×10^{31}	U18, CV2	0.6 -1.8
X4	17:40:41.53	-53:40:26.4	2.0''	1.3 ± 0.5	3.6×10^{31}	CV5	0.7 -0.1
X5	17:40:41.36	-53:40:02.0	1.2''	3.0 ± 0.6	8.2×10^{31}	U24	0.0 0.0
X6	17:40:40.4	-53:40:18	∞ ^b	0.4	< 1.1×10^{31}	U43	0.8 2.8

^a Unabsorbed luminosities listed in the 0.5–2.5 keV band, for a cluster distance of 2.2 kpc, and column density of 1.0×10^{21} cm⁻². For best fit (*Chandra*) column densities and bremsstrahlung spectra for individual sources, see Grindlay et al. (2001a).

^b The 2σ confidence radius of the position of X6 is infinite, because the K-S probability that the model and the image represent the same parent distribution is always above 5 per cent, regardless of the source location.

^c U18, U24 and U43 are Grindlay et al. (2001a) *Chandra* IDs. U18 also identified as either a BY Dra or MSP by Grindlay et al. (2001a), and U43 identified as a BY Dra binary by Taylor et al. (2001). CV2 first identified as Hα object by Cool et al. (1995).

^d Offset between the given positions (subscript *R*) and the ones listed in Grindlay et al. (2001a, subscript *C*). A boresight offset ($\Delta\alpha_{R-C} = 4.9$ pix and $\Delta\delta_{R-C} = 4.6$ pix) has been applied to match the positions of our best-constrained source (X5) and its *Chandra* counterpart (U24). When the emission from two *Chandra/HST* sources corresponds to a single *ROSAT* source, the latter has been associated with the mean position of the *Chandra/HST* sources.

moderately crowded fields. After comparing results from the IRAF implementations of the Maximum Entropy Method, the L-R algorithm (both applicable primarily to optical images), and from CLEAN (used mostly in radio imaging), we found that L-R deconvolution (Lucy 1974; Richardson 1972) most reliably discerns the five-source distribution found by our iterative source-modelling scheme (Section 5). The positions of the peaks in the deconvolved image are in excellent agreement (to within ± 1 pix = ± 0.5 arcsec) with the K-S best-fit source positions, which exemplifies the usefulness of L-R deconvolution in analysing crowded fields. Unfortunately, the L-R method does not provide a measure of the goodness of fit of these positions and of the significance of the peaks in the reconstructed image. These need to be determined separately with a multi-source fitting routine (since the field is crowded), such as DAOPHOT/ALLSTAR, or the current (2D K-S) iterative method. Furthermore, the obtained intensities of the deconvolved sources are in much poorer agreement with the ones from the 2D K-S best-fit model. Nevertheless, L-R deconvolution does give an indication for the existence of more than 3 sources (which could not be determined with the source-searching methods). The L-R method thus provides a very good initial guess for the source configuration, which can be input to iterative source-modelling algorithms.

DAOPHOT/ALLSTAR: The DAOPHOT package is designed for the analysis of crowded optical images, and as such it assumes that the images are in the Gaussian statistics (high number of counts per pixel) regime. Thus, strictly speaking, the package is inapplicable to data governed by Poisson statistics, such as most x-ray images (including our NGC 6397 image, containing ≤ 3 counts per pixel), because it severely underestimates random errors. However, until recently DAOPHOT was the only widely available software for reduction of crowded fields, and it has been suggested (Cool et al. 1993) that it can be useful for analysing crowded x-ray fields.

Our experience with ALLSTAR is that it is heavily dependent on several loosely defined parameters which, in regimes of severe source confusion and low signal-to-noise as in our

NGC 6397 image (Figure 5), critically determine the performance of the task. We found that different combinations of the values of the parameters and of the initial guess for the source distribution produced different final results, in which the number of detected sources in the NGC 6397 image varied from 2 to 5. By judiciously adjusting its parameters, ALLSTAR can be made to detect 5 sources, however that combination is not favoured statistically over other combinations with fewer sources. In the case when ALLSTAR detects 5 sources, the obtained positions and intensities are such that the K-S probability of similarity with the *ROSAT* image is < 1 per cent ($Z_n = 2.2$).

Maximum Likelihood: Given our method of optimisation – minimising the maximum residual D_{\max} (albeit we then further minimise the K-S statistic Z_n) – ML analysis would be expected to produce a similar fit. This is indeed the approach of Verbunt & Johnston (2000) in analysing the same *ROSAT* field. The results for the 5 detected sources (Model I in (Verbunt & Johnston 2000); X1–X5 in this paper) agree well; in addition, our analysis suggests the possible presence of the faint source X6. We choose to employ a 2D K-S test to assess the goodness of fit instead, banking on its sensitivity to diffuse distributions. As pointed out by the referee, it is a good test for the location of smeared objects, but it is rather insensitive to their width. Via K-S, a source may be deduced to be unresolved, despite having broader profile, which can frequently be the case in Poisson noise limited images.

We have thus demonstrated that under conditions of severe source confusion and low *S/N*, our source-detection method based on a 2D K-S test works better than other available techniques. We attribute its performance to the fact that our approach uses the actual PSF in searching for sources (sliding-cell and wavelet detect algorithms do not), that no information is lost to binning (as in the Pearson χ^2 test, used in ALLSTAR), and that it is more sensitive to broad emission than other tests (e.g., ML).

We have not made a comparison of our method against the Pixon deconvolution method (Pina & Puetter 1993). Our method was originally intended to enhance sensitivity for crowded point source detection; the Pixon method also

shows good results for the detection of low surface brightness features.

7 DISCUSSION

7.1 Applicability to distributions with unknown parameters

Rigorously, the presented look-up Table 3 (generated by comparing simulations of models with *a priori* known parameters) is not applicable when comparing an image of an unknown source distribution to a simulation with known parameters. Lilliefors (1967) investigates this situation for the case of the 1D K-S test and sampling from a distribution with unknown mean and variance (“the Lilliefors test for Normality”). He finds that the standard 1D K-S test table is *too conservative*, i.e. with an appropriately generated look-up table (via Monte Carlo simulations), one can reject the null hypothesis that a sampled distribution is Normal at a higher significance level than with the standard table.

The implications of this to our case are not known, and have not been investigated. Speculatively extrapolating Lilliefors’s conclusion, the 2D K-S test for comparing an unknown to a known distribution should be, if anything, more powerful than presented. This would increase the significance of source X6, making its association with the suggested BY Dra variable more likely.

The advantage of an ML approach here would be that likelihood ratios between different models do not suffer from such problems.

7.2 Significance of the detections

The developed detection significance test for additional sources in Section 4.2 may seem subjective, since prior knowledge is needed about the $Z_n^{M,M}$ curve (where M is the number of sources in the image). Naturally, this information is not available when working with an astronomical image representing an unknown source distribution, where M is a sought parameter. However, due to the (nearly) distribution-free character of the pseudo one-sample 2D K-S test (Section 3.1.2), all that is needed is the correlation coefficient CC of the counts in the image, which is readily available ($CC = 0.17$ for the *ROSAT* image in Figure 5). Provided that the best-fit model with N sources represents the image reasonably well (K-S probability $\gtrsim 1$ per cent), the $Z_n^{N,N}$ curve will be indistinguishable from the $Z_n^{M,M}$ curve of the image, since the correlation coefficients of the N -source model and of the (M -source) image will be very similar. Indeed, in our case the best-fit five-source model has $CC = 0.19$, which given the slow dependence of the Z_n distribution on CC , well approximates the Z_n distribution for $CC = 0.17$ (the correlation coefficient of the counts in the *ROSAT* image).

More general than the false-detection probability is the fraction P'_K of cases, in which the observed image can be represented by a best-fitting model containing $K < N \leq M$ sources, where K does not necessarily equal $M - 1$. Here N is our best guess for the number of sources in the image, and M is the actual (unknown) number of sources. The quantity $1 - P'_K$ is the significance level at which we can reject

the hypothesis that the image contains only K sources. To determine P'_K using the 2D K-S test, we need to compare multiple images of the same field to a single model simulation with K sources (Section 3.1.2). Naturally, this cannot be done, since there rarely exist multiple available images of the same field. However, P'_K is well approximated by the quantity $P_{K,N}$, given that, as discussed above, $Z_n^{N,N}$ describes well the $Z_n^{M,M}$ distribution of the image. This is the value listed in Table 5 (using $N = 5$) for the probability that the *ROSAT* image can be fitted with fewer than 5 sources. For $K = N - 1$, in $P_{K,N}$ we recover the false-detection probability for the N th source, as already discussed in Section 4.2.

7.3 Detected sources

The positions and the count rates of the detected sources are in excellent agreement with Model I (based on 1995 *ROSAT* data) of Verbunt & Johnston (2000) in their maximum-likelihood analysis of the same HRI field. A *Chandra* image of the core region of NGC 6793 (Grindlay et al. 2001a) reveals a greater complexity of sources (Figure 6). The source “doubles” CV1 and CV4, as well as CV2 and U18 are too close (~ 2.5 arcsec ≈ 0.3 FWHM) to be distinguished as separate sources in the *ROSAT*/HRI image, and are represented as blended sources X1 and X4, respectively. The remainder of the sources marked with open squares are too faint ($L_x < 10^{31}$ erg s $^{-1}$ Grindlay et al. 2001a) to be detected given the crowdedness of the field. None the less, there is a clear one-to-one correspondence between the brightest ($L_x > 10^{31}$ erg s $^{-1}$) *Chandra* sources, and the ones detected in the *ROSAT*/HRI image using the 2D K-S technique.

Although in their Model IV Verbunt & Johnston predict the existence of separate x-ray counterparts to sources CV2 and U18, that model is fit to 1991 *ROSAT*/HRI data when CV2 was more prominent in x-rays relative to U18 (hence could be more accurately centred; cf. Fig. 1 in Cool et al. 1993), and three of the sources in the model have fixed positions. On the other hand, in our 2D K-S test iterative analysis we have not used any fixed parameters. Moreover, the K-S test suggests the existence of source U43, detected (albeit inconclusively, and offset by ~ 4.5 arcsec from its *Chandra* position) as source X6, for which there exists no x-ray identification prior to the *Chandra* results of Grindlay et al. (2001a). Although the source is fainter ($\log L_x = 29.4$ Grindlay et al. 2001a) than other undetected sources in the complex X1–X4, the source must have been $\gtrsim 10\times$ brighter to have been detectable with *ROSAT* (indeed, BY Dra binaries were discovered in globular clusters as faint and flaring x-ray sources, Grindlay et al. 2001b).

8 CONCLUSION

We have developed an application of the 2D K-S test (Peacock 1983; Fasano & Franceschini 1987) in a source-detection algorithm for astronomical images. By employing the “sub-pixelization” technique on 3D astronomical images, we show that the 2D K-S test has greater power than the 3D K-S test – the intuitive choice for such images. We use Monte Carlo integration to determine the cumulative values of the proposed model distribution in all four quadrants around each count and, recognising the deviations that this incurs from

the derived Z_n distributions, we provide our own reference tables for estimating the K-S probability.

We devise an iterative source-modelling routine that employs the K-S probability as a goodness of fit estimator, and can be used to find the optimum number, positions, and intensities of blended sources. We then apply the iteration scheme to a deep (75 ksec) *ROSAT*/HRI exposure of the core region of NGC 6397 and find five blended sources, as well as a possible sixth one. The locations of the five brightest (and possible sixth) x-ray sources match closely (within the positional error bars) the locations of probable CVs and BY Dra systems, discovered with *HST* (Cool et al. 1993, 1995; Taylor et al. 2001), and confirmed with *Chandra* (Grindlay et al. 2001a). The sixth source, X6, is a marginal detection with the 2D K-S technique and is likely identified with the much fainter *Chandra* source, U43 (Grindlay et al. 2001a), which is in turn identified with a BY Dra binary, PC-4 (Taylor et al. 2001).

Comparisons to other source-detection schemes (sliding-cell, wavelet detect, DAOPHOT/ALLSTAR, L-R deconvolution and ML techniques) applied to the same image demonstrate the superior power of our method in heavily crowded fields with low signal-to-noise. The example with the *ROSAT*/HRI deep field indicates that the proposed iterative source-modelling scheme can find applications in small-number statistics high-energy imaging, e.g. in deep exposures of globular clusters and extragalactic nuclear regions with *Chandra*, where the size of the PSF is often comparable to the angular separation between the objects.

We thank our collaborators Adrienne Cool and Peter Edmonds for numerous discussions. This research was partially supported by NASA/LTSA grant NAG5-3256 and by *HST* grant GO-06742.

REFERENCES

Becker, W., Trümper, J. 1999, *A&A*, 341, 803.

Cool, A.M., Grindlay, J.E., Krockenberger, M., and Bailyn, C.D. 1993, *ApJ Letters*, 410, L103.

Cool, A.M., Grindlay, J.E., Cohn, H.N., Lugger, P.M., and Slavin, S.D. 1995, *ApJ*, 439, 695.

Cool, A.M., Grindlay, J.E., Cohn, H.N., Lugger, P.M., and Bailyn, C.D. 1998, *ApJ Letters*, 508, L75.

Damiani, F., Maggio, A., Micela, G., and Sciortino, S. 1997, *ApJ*, 483, 350.

Djorgovski, S.G., Meylan, G. 1993, in Djorgovski, S.G., Meylan, G., eds, *Structure and dynamics of globular clusters*, ASP Conf. Ser. Vol. 50, ASP, p. 373.

Edmonds, P.E., Grindlay, J.E., Cool, A.M., Cohn, H.N., Lugger, P.M., and Bailyn, C.D. 1999, *ApJ*, 516, 250.

Fasano, G., Franceschini, A. 1987, *MNRAS*, 225, 155.

Freeman, P.E., Kashyap, V., Rosner, R., and Lamb, D.Q. 2001, in Babu, G.J., Feigelson, E.D., eds, *Proceedings of Statistical Challenges in Modern Astronomy III* (New York: Springer-Verlag), in press (and available at <http://arXiv.org/abs/astro-ph/0108429>).

Gosset, E. 1987, *A&A*, 188, 258.

Grindlay, J.E. 1999, *Magnetic CVs in Globular Clusters*, ed. Hellier, C. and Mukai, K., ASP Conference Series, vol. 157, p.377.

Grindlay, J.E., Heinke, C.O., Edmonds, P.D., Murray, S.S., Cool, A.M. 2001, *ApJ Letters*, 563, 53.

Grindlay, J.E., Heinke, C.O., Edmonds, P.D., Murray, S.S., 2001, *Science*, 292, 2290.

Hanish, R. 1995, *IRAF/LUCY* help file.

Harris, D.E. 1999a, AAS HEAD meeting #31, #17.12, The *ROSAT*/HRI: The Last Hurrah! (a.k.a. How to get better images).

Harris, D.E. 1999b, The HRI Bug for Aspect Time, <sao-ftp.harvard.edu://pub/rosat/dewob/asptime.doc> .

Harris, D.E., Prestwich, A., Primini, F.A., Silverman, J.D., Snowden, S.L. rev. 1997, The *ROSAT* High Resolution Imager (HRI) Calibration Report, U.S. *ROSAT* Science Data Center/SAO.

Harris, D.E., Silverman, J.D., and Hasinger, G., 1998a, Spatial Corrections of *ROSAT*/HRI Observations from Wobble-related Aspect Problems, U.S. *ROSAT* Science Data Centre/SAO.

Harris, D.E., Silverman, J.D., Hasinger, G., and Lehman, I. 1998b, *A&A Suppl.*, 133, 431.

Hertz, P., Grindlay, J.E. 1983, *ApJ*, 275, 105.

Kendall, M.G., Stuart, A. 1979, *The Advanced Theory of Statistics*, Griffin, London.

Lilliefors, H. 1967, *J.Am.Stat.Assoc.*, 62, 399.

Lucy, L.B. 1974, *AJ*, 79, 745.

Metchev, S.A. 1999, Sr. Thesis, Harvard College.

Peacock, J.A. 1983, *MNRAS*, 202, 615.

Pina, R.K., Puetter, R.C. 1993, *PASP*, 105, 630.

Press, W., Teukolski, S., Vetterling, W., Flannery, B., *Numerical Recipes in C: The Art of Scientific Computing*, Cambridge University Press, 1997, p.645.

Richardson, W.H., J. Opt. Soc. Am., 62, 55.

Stetson, P.B. 1987, *PASP*, 99, 191.

Stetson, P.B. 1991, in *ESO/ST-ECF Data Analysis Workshop*, P.J. Grosboel and R.H. Warmels, eds., ESO Conf. and Workshop Proc. No. 38, p.187.

Taylor, J.M., Grindlay, J.E., Edmonds, P.D., Cool, A.M. 2001, *ApJ*, 553, 169.

Verbunt, F., Johnston, H.M. 2000, *A&A*, 358, 910.